Modeling Local and Advective Diffusion of Fuel Vapors to Understand Aqueous Foams in Fighting Fires

Final Report

Author:
Andrew Brandon
asbrando@math.umd.edu

Advisor:
Dr. Ramagopal Ananth
Naval Research Laboratory, Washington, D.C.
ramagopal.ananth@nrl.mil

Abstract

The purpose of this project was to investigate fuel vapor suppression by aqueous film and foam layers. Immediately after application, aqueous film and foam layers have the effect of suppressing fuel evaporation, however this suppression is not constant over time. If enough time elapses, the fuel vapor concentration above the film and foam layers can reach levels characteristic of an uncovered fuel pool. This can allow for re-ignition of the original fire. Experiments done by Leonard and Williams have studied this phenomena. It is unknown how the fuel moves through the film or foam layers and the purpose of this project was to model that movement by assuming that the fuel dissolves and diffuses through the aqueous layer. In addition to delivering a model that can simulate these experiments, I promised that this model would be capable of finding an effective diffusion constant D_F for the foam and film. This would be done by minimizing the residual between the experimental and numerical results. In order to ensure that the model was correctly simulating the experiments, the model was extensively validated. After validation, the model was applied to test cases and film layer data collected by Leonard. After analyzing the results of simulating Leonard's experiment, it appears that the dissolution and diffusion transport mechanism is not the primary transport mechanism of fuel through the film layers.

1 Background

To combat fuel pool fires, the United States Navy employs several types of fluorinated fire fighting foams. Once applied to a pool fire, a portion of the liquid in the foam drains over a short period of time, depositing a layer of film on top of the fuel pool. The fluorine surfactant in the foam is responsible for decreasing the surface tension of the foam solution, allowing the aqueous layer to"float" on the surface of the fuel pool. This film suppresses further evaporation of the fuel. However, several experiments have shown that this suppression of fuel vapors is not constant over time.

In the 1970s, Dr. Joseph Leonard et al at the Naval Research Laboratory (NRL) in Washington, D.C. began testing the suppression ability of the then new aqueous film forming foam (AFFF) [1]. To test AFFF, they took the film that the foam creates and placed a specified amount on a fuel pool. Then they measured the concentration of fuel vapors over a specified amount of time. Their results confirmed that the film created by AFFF was capable of initially suppressing the vapors of several fuel types [1]. What they did not expect to find was that after the initial suppression, the concentration of fuel vapors increased with time. In some cases, fuel vapor concentrations reached levels characteristic of when foam is absent. Recently, this phenomenon has gained interest.

Dr. Bradley Williams, also of NRL, is currently working on an experiment similar to Dr. Leonard's. His experiment involves placing an aqueous foam layer on the surface of a fuel pool rather than the film layer. When measuring fuel vapor concentration levels over a period of time, Dr. Williams has also found that the concentration of fuel vapor increases with time after the initial suppression by the foam layer. Figure 1 is a depiction of the application of an aqueous foam and the resulting film and foam layers.

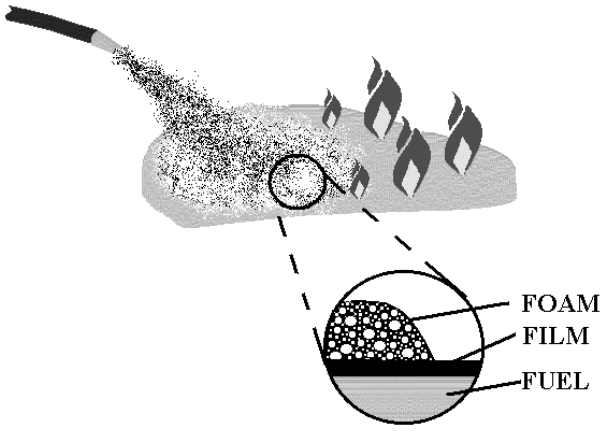

Figure 1: Application of an aqueous foam with foam and film layer formation on a fuel pool [2].

The exact mechanisms of fuel transport through foam or film layers are not known. However, there are currently two main hypotheses. The first is that the fuel vapors are able to dissolve in the aqueous solution and then diffuse throughout the solution. The second theory is that the fuel is able to emulsify into the aqueous solution and then is transported to the surface due to density differences. How fuel is transported and by which of these two mechanisms were the driving questions behind this project.

To answer this question, I modeled the experiments of Leonard and Williams by simulating either a film or foam layer on the surface of the fuel pool. The case of a foam layer on the surface of a film layer was not considered. To model the transport of fuel vapors through the layers, I assumed that the transport mechanism was that of dissolution and diffusion. This diffusion would be governed by an effective diffusion coefficient D_F and D_F was found by minimizing the residual between the experimental and numerical results. Once the value of D_F capable of reproducing the experimental data was found, it would be analyzed to determine if our transport mechanism assumption was correct.

2 The Model

The experiments of Leonard and Williams involved a cylindrical container that was $20cm$ in height and $2.5cm$ in radius. A fuel pool was placed in the bottom of the container and then a film or foam layer was placed on the surface of the fuel pool so that the fuel pool was completely and uniformly covered. Above the film or foam layer is a fritted glass disk that was attached to a pipe that runs out the top of the container. Pure nitrogen was then blown through the pipe and fritted glass disk at a constant velocity. The flow of nitrogen then move across the film or foam layer surface, entraining any fuel vapors. The flow would then move through an outlet at the top of the container to be analyzed. See Figure 2 for a depiction of the experimental domain.

Since the experimental domain is cylindrical and axisymmetric, the model domain will be the region outlined in red in Figure 2. The two domains that were modeled were the film or foam layer and the gas domain within the red box. These two domains are labeled Domain 1 and Domain 2 within the figure and the fuel pool was represented as the bottom boundary condition in Domain 2. The flow rates that were used within the experiments were chosen such that the film or foam layer was undisturbed so the film and foam layers were assumed to be stationary in the model. Also, since the concentration of fuel vapors in Domains 1 and 2 is small, the change in density in the gas of the container will also be small. Thus, the density of the container will be assumed to be homogenous and constant, which leaves us with an incompressible system. The third assumption in the model is that the fuel vapors will be transported through the film or foam layer by dissolution and diffusion.

In order to model these experiments, the axial and radial velocities of Domain 1

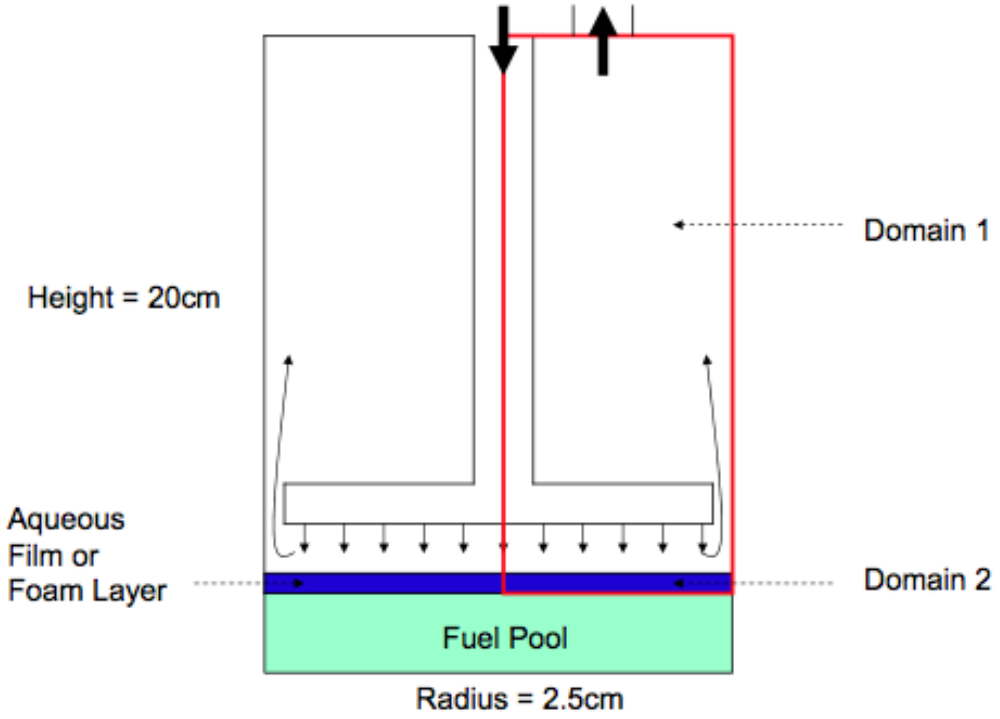

Figure 2: A slice of the experimental domain from the top of the container to the bottom.

and the concentration of fuel vapors in Domains 1 and 2 must be found. Thus, the species fraction equation (1) and the Navier-Stokes equation (2) will be solved. In equations (1) and (2), Y is the mole fraction

$$\frac{\partial Y}{\partial t} + \nabla \cdot (vY) = D\nabla^2(Y) \tag{1}$$

$$\frac{\partial v}{\partial t} + v \cdot \nabla(v) = \frac{-1}{\rho}\nabla(P) + \eta\nabla^2(v) \tag{2}$$

or mass fraction (depending on the bottom boundary condition) of fuels vapors and $v \equiv (u, w)$ where u is the radial velocity and w is the axial velocity [4]. Note that the gravity term in the Navier-Stokes equation has been removed. Gravity has been removed because there are no density perturbations in the system and gravity serves to create flow due to density differences. Now, after applying the assumption of incompressibility ($\nabla \cdot v = 0$) and applying the differential operators in axisymmetric cylindrical coordinates, equations (1) and (2) transform into

$$\frac{\partial Y}{\partial t} + u\frac{\partial Y}{\partial r} + w\frac{\partial Y}{\partial z} = D\Big(\frac{\partial^2 Y}{\partial r^2} + \frac{1}{r}\frac{\partial Y}{\partial r} + \frac{\partial^2 Y}{\partial z^2}\Big) \tag{3}$$

$$\frac{\partial u}{\partial t} + u\frac{\partial u}{\partial r} + w\frac{\partial u}{\partial z} = \frac{-1}{\rho}\frac{\partial P}{\partial r} + \eta\Big(\frac{\partial^2 u}{\partial r^2} + \frac{1}{r}\frac{\partial u}{\partial r} + \frac{\partial^2 u}{\partial z^2}\Big) \tag{4}$$

$$\frac{\partial w}{\partial t} + u\frac{\partial w}{\partial r} + w\frac{\partial w}{\partial z} = \frac{-1}{\rho}\frac{\partial P}{\partial z} + \eta\Big(\frac{\partial^2 w}{\partial r^2} + \frac{1}{r}\frac{\partial w}{\partial r} + \frac{\partial^2 w}{\partial z^2}\Big) \tag{5}$$

To solve equation (3) for the concentration (mole or mass fraction) Y, it is necessary to know D. There will be two values for D, one value for Domain 1, D_A, and another for Domain 2, D_F. The value for D_A represents the diffusivity of fuel vapors in N_2 and can be estimated using kinetic theory. The second value D_F represents the diffusivity of fuel vapors in the film or foam and this value is unknown. This value, D_F, was found by comparing the numerical model to experimental data. In order to solve equations (4) and (5) for u and w, it is necessary to solve for pressure, P. Solving for pressure is extremely computationally expensive and determining boundary conditions for pressure can be ambiguous. Thus, to avoid having to solve for pressure, the stream function and vorticity transformation were used on equations (4) and (5). The substitutions required for this transformation are $u = \frac{-1}{r}\frac{\partial \psi}{\partial z}$, $w = \frac{1}{r}\frac{\partial \psi}{\partial r}$, and $\Omega = \frac{\partial u}{\partial z} - \frac{\partial w}{\partial r}$ where ψ is the stream function and Ω is vorticity [5,7]. Upon inserting these substitutions, equations (4) and (5) are transformed into the stream function and vorticity equations. Note that in these transformed equations there is no pressure term, P.

$$\Omega = \frac{1}{r^2}\frac{\partial \psi}{\partial r} - \frac{1}{r}\frac{\partial^2 \psi}{\partial r^2} - \frac{1}{r}\frac{\partial^2 \psi}{\partial z^2}$$

$$\frac{\partial \Omega}{\partial t} + u\frac{\partial \Omega}{\partial r} + w\frac{\partial \Omega}{\partial z} = \frac{u\Omega}{r} + \eta\Big(\frac{\partial^2 \Omega}{\partial r^2} + \frac{1}{r}\frac{\partial \Omega}{\partial r} + \frac{\partial^2 \Omega}{\partial z^2} - \frac{\Omega}{r^2}\Big)$$

This transformation leaves us with having to solve equations (6), (7), and (8) in Domain 1, where $u = \frac{-1}{r}\frac{\partial \psi}{\partial z}$, $w = \frac{1}{r}\frac{\partial \psi}{\partial r}$, and D_A is the diffusion coefficient for fuel vapors in pure nitrogen N_2. Then in Domain 2, only equation (9) needs to be solved, where D_F is defined as the effective diffusion coefficient for fuel vapors in the film or foam layer. Equation (9) has no convective terms because the film or foam layer is assumed to be stationary, which leads to $u = w = 0$ in Domain 2.

$$\frac{\partial Y}{\partial t} + u\frac{\partial Y}{\partial r} + w\frac{\partial Y}{\partial z} = D_A\Big(\frac{\partial^2 Y}{\partial r^2} + \frac{1}{r}\frac{\partial Y}{\partial r} + \frac{\partial^2 Y}{\partial z^2}\Big) \tag{6}$$

$$\Omega = \frac{1}{r^2}\frac{\partial \psi}{\partial r} - \frac{1}{r}\frac{\partial^2 \psi}{\partial r^2} - \frac{1}{r}\frac{\partial^2 \psi}{\partial z^2} \tag{7}$$

$$\frac{\partial \Omega}{\partial t} + u\frac{\partial \Omega}{\partial r} + w\frac{\partial \Omega}{\partial z} = \frac{u\Omega}{r} + \eta\Big(\frac{\partial^2 \Omega}{\partial r^2} + \frac{1}{r}\frac{\partial \Omega}{\partial r} + \frac{\partial^2 \Omega}{\partial z^2} - \frac{\Omega}{r^2}\Big) \tag{8}$$

$$\frac{\partial Y}{\partial t} = D_F\Big(\frac{\partial^2 Y}{\partial r^2} + \frac{1}{r}\frac{\partial Y}{\partial r} + \frac{\partial^2 Y}{\partial z^2}\Big) \tag{9}$$

3 Solution Algorithms

The solutions for equation (6), (7), (8), and (9) were found using a series of finite difference algorithms. To solve (6), (8), and (9), an upwind differencing algorithm for convective diffusive equations presented in [6] was implemented. This algorithm calls for backwards differencing to be applied to the convective terms and centered differencing to be applied to the diffusive terms. This algorithm has a restraint on the timestep, $\triangle t$, that could be used to discretize the time derivative. This restraint is

$$\triangle t < \frac{1}{\frac{4D}{\tau} + \frac{max(u)}{\triangle r} + \frac{max(w)}{\triangle z}}$$

where $max(u)$ and $max(w)$ are defined to be the maximum radial and axial velocities in the model domain respectively and $\tau \equiv \min(\triangle r^2, \triangle z^2)$ [6]. The model was designed such that the equations in both Domains 1 and 2 were solved using the same timestep value, $\triangle t$, but because there was a different D and $\triangle z$ value in Domains 1 and 2, the timestep had to be designed such that the upwind differencing scheme was stable in both domains. Thus, the D and $\triangle z$ values that were chosen to find $\triangle t$ were the D and $\triangle z$ values that resulted in the smallest timestep. This ensured that the upwind differencing scheme was stable in both domains.

Equation (7) involves no time derivative so it could not be solved in a manner similar to the other equations. To solve equation (7), a successive over-relaxation, SOR, algorithm was implemented. The SOR algorithm is an iterative solver and is similar to the Gauss-Seidel method except that SOR uses a relaxation parameter to achieve faster convergence. To find the optimal relaxation parameter, Chebyshev acceleration was implemented in tandem with the SOR algorithm. Chebyshev acceleration recalculates the relaxation parameter at each iteration of the SOR algorithm such that it is the optimal relaxation parameter for that iteration. This guarantees that the SOR solver converges as rapidly as possible. The successive over-relaxation with Chebyshev acceleration algorithm that was used in the model was the algorithm presented in [8]. Centered differencing was used to discretize (7) and the solution was iterated upon following the iteration formula in [8]. Once the residual of the solution field fell beneath a prescribed tolerance, the solution was presumed to have been found. For further information on the implementation of the SOR with Chebyshev acceleration algorithm within this model, please see the December 2011 progress report.

Once the solution algorithms had been chosen, it remained to couple the solvers. The algorithm for doing this and finding the solutions for u, w, ψ, and Ω at each timestep was presented in [6]. This algorithm called for boundary conditions on ψ to be derived from those on u and w and for the remaining boundary conditions on u and w to be implemented within the code. Boundary conditions for Ω are then determined numerically from the u and w solution fields according to the vorticity definition $\Omega = \frac{\partial u}{\partial z} - \frac{\partial w}{\partial r}$. Normally, boundary conditions on Ω would be derived from boundary conditions on u and w, however this algorithm calls for the boundary conditions on Ω to be found numerically. Letting the solutions for u, w, ψ, and Ω at the n^{th} timestep be u^n, w^n, ψ^n, and Ω^n, then the algorithm for finding u^{n+1}, w^{n+1}, ψ^{n+1}, Ω^{n+1}, and Y^{n+1} is as follows.

1. Determine the boundary conditions on Ω^n numerically using the u^n and w^n fields and $\Omega = \frac{\partial u}{\partial z} - \frac{\partial w}{\partial r}$.

2. Find Ω^{n+1} with the upwind differencing algorithm.

3. Find ψ^{n+1} using SOR with Chebyshev acceleration. There is an Ω term in (7), however only the interior points of Ω^{n+1} are required to find ψ^{n+1}.

4. Solve for u^{n+1} and w^{n+1} from ψ^{n+1}.

5. Solve for Y^{n+1} using u^{n+1}, w^{n+1}, and the upwind differencing algorithm.

4 Validation

Simplified Domain

Once the solution algorithms were implemented, it remained to check that they were done so correctly. Validation was begun on a simplified domain. This domain was an axisymmetric cylindrical container like the experimental domain but without the pipe and fritted glass disk. Once the simplified domain was in place, work began on validating the species fraction solver (i.e. the routine responsible for solving equations (6) and (9)).

The first case that was tested was a pure advection case with only axial dependence. This corresponds to the equation

$$\frac{\partial Y}{\partial t} + c\frac{\partial Y}{\partial z} = 0$$

which has the analytical solution of

$$Y(z,t) = \left\{ \begin{array}{ll} 0 & \frac{z}{c} > t \\ 1 & \frac{z}{c} \leq t \end{array} \right\}$$

for an initial condition of $Y(z,0) = 0$, a boundary condition of $Y(0,t) = 1$, and a uniform axial velocity c inside the container. To implement this case of pure advection within the code, the appropriate initial and boundary conditions were implemented along with a small diffusion coefficient. This had the effect of making the diffusion terms small without having to remove those terms from the code. The diffusion coefficient that was chosen was $D = 10^{-4}\frac{cm^2}{s}$ and the flow speed c was $4\frac{cm}{s}$. The residual between the numerical and analytical solution fields was then taken and Figure 3 is a plot of that residual field. Looking at Figure 3, one can see a region where the residual is fairly high. This region is the interface between $Y = 0$ and $Y = 1$. Within the analytical solution this region is sharp however finite differencing is unable to capture sharp interfaces. Finite differencing will cause this sharp interface to become smooth and one can see evidence of this within Figure 3. Because the residual goes to zero in all other regions, the species fraction solver is working correctly for the pure advection case.

The second case that was tested was a pure diffusion case with only axial dependence. This corresponds to the equation

$$\frac{\partial Y}{\partial t} = D\frac{\partial^2 Y}{\partial z^2}$$

which has the analytical solution of

$$Y(z,t) = 1 - \sum_{n=0}^{\infty} \frac{4}{\pi(2n+1)} e^{-D(\frac{\pi(2n+1)}{40})^2 t} \sin\left(\frac{\pi(2n+1)}{40} z\right)$$

for an initial condition of $Y(z,0) = 0$ and boundary conditions of $Y(0,t) = 1$ and $\frac{\partial Y}{\partial z} = 0$ at $z = 20$. The implementation of pure diffusion within the code was a much more exact task and was accomplished by setting $u = w = 0\frac{cm}{s}$. The diffusion coefficient that was used in the analytical and numerical solutions was $D = 0.25\frac{cm^2}{s}$. Figure 4 is a plot of the residual between the analytical and numerical solutions for $D = 0.25\frac{cm^2}{s}$ and $w = 0\frac{cm}{s}$ at time=$1.5s$. Looking at Figure 4, one can see that the solutions are much more in agreement since the residual is on the order of 10^{-5}. Again, this is due to the solution being smooth which allows finite differencing to capture it. Because the solver found the correct solution to the pure diffusion case, in addition to the pure advection case, one can conclude that the species fraction works correctly.

Once the species fraction solver was validated, the vorticity solver was then tested. Comparing equations (6) and (8), one can see that the equations are very similar except for two terms in equation (8). These two terms require no discretization, so to test the

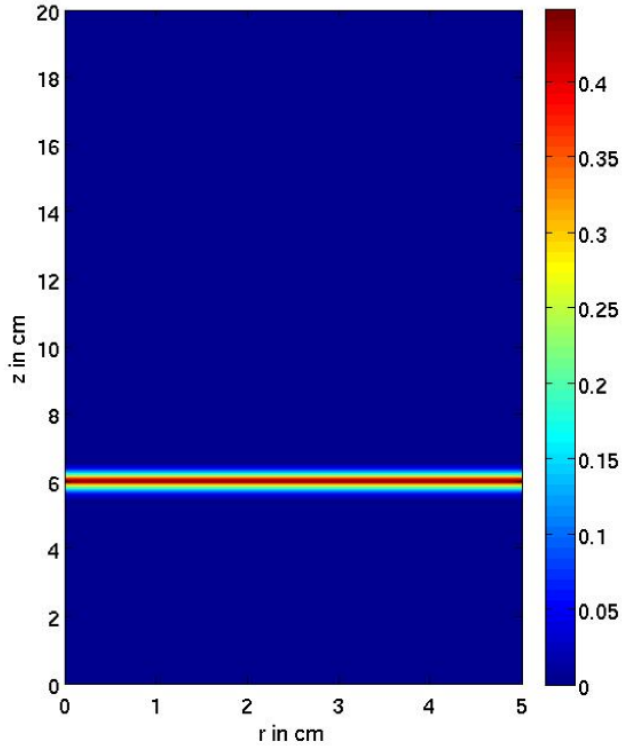

Figure 3: Residual between numerical and analytical solution for pure advective flow for $D = 10^{-4} \frac{cm^2}{s}$ and $c = 4 \frac{cm}{s}$ at time=1.5s.

vorticity solver, these two terms were removed. In addition, the boundary conditions in the species fraction solver were implemented in the vorticity solver and η was set equal to D. This had the effect of solving for the species fraction manifested as vorticity. Once this was done, a residual between the two solutions was taken. If the vorticity solver was correctly implemented, then the two solutions would be similar. In fact, the residual between the two was found to be machine accuracy. Thus, the vorticity solver is correctly discretized and has been validated.

The last solver that needed to be validated was the stream-function solver. This solver is different in nature to the upwind differencing scheme so it could not be compared to the species fraction solver like the vorticity solver could. In the end, the stream function solver was validated by comparing solutions from the SOR algorithm to Matlab's finite element solver. A series of the boundary conditions were implemented for both numerical solvers and then the residual was taken between the two solutions. The residual was consistently on the order of 10^{-4} so the discretization and SOR algorithm were correctly implemented. With the three solvers being validated, the experimental domain was then

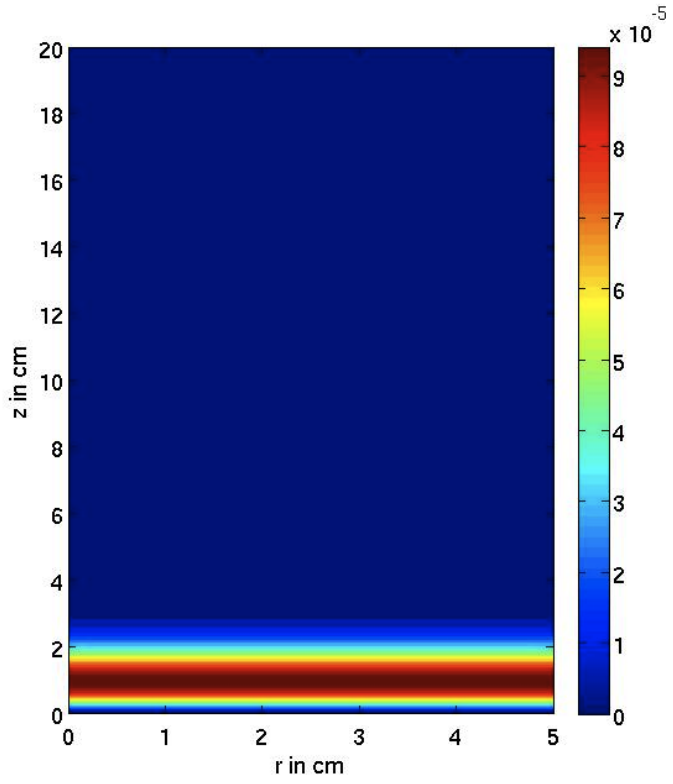

Figure 4: Residual between numerical and analytical solution for pure advective flow for $D = 10^{-4}\frac{cm^2}{s}$ and $c = 4\frac{cm}{s}$ at time=1.5s.

added. Once the solvers were coupled, further validation began.

Experimental Domain

Designing the experimental domain involved adding the pipe and fritted glass disk to Domain 1. This also required the derivation of new boundary conditions on ψ. Table 1 is a list of the boundary conditions corresponding to the labeled boundaries in Figure 5. Several values in Table 1 need to be discussed before continuing. The value Y_{sur} is the mole or mass fraction of fuel vapors in air due to the vapor pressure of the fuel. The value of α is $\frac{-c}{2}2.25^2$ since the width of the fritted glass disk is $2.25cm$ and the value of c is the input flow speed. The boundary condition for Y on boundary 9 is a no flux boundary condition.

Boundary	Y	u	w	ψ (derived from)
1	$Y = Y_{sur}$	$u = 0$	$w = 0$	$\psi = 0(w = 0)$
2	$\frac{\partial Y}{\partial r} = 0$	$u = 0$	$w = 0$	$\psi = 0(u = 0)$
3	$\frac{\partial Y}{\partial z} = 0$	$u = 0$	$w = 0$	$\psi = 0(w = 0)$
4	$\frac{\partial Y}{\partial z} = 0$	$\frac{\partial u}{\partial z} = 0$	$\frac{\partial w}{\partial z} = 0$	$\frac{\partial^2 \psi}{\partial z^2} = 0(\frac{\partial u}{\partial z} = 0)$
5	$\frac{\partial Y}{\partial z} = 0$	$u = 0$	$w = 0$	$\psi = \alpha(w = 0)$
6	$\frac{\partial Y}{\partial r} = 0$	$u = 0$	$w = 0$	$\psi = \alpha(u = 0)$
7	$\frac{\partial Y}{\partial z} = 0$	$u = 0$	$w = 0$	$\psi = \alpha(w = 0)$
8	$\frac{\partial Y}{\partial r} = 0$	$u = 0$	$w = 0$	$\psi = \alpha(u = 0)$
9	$\rho Y w + D\rho \frac{\partial Y}{\partial z} = 0$	$u = 0$	$w = c$	$\psi = \frac{-c}{2} r^2 (w = c)$
10	$\frac{\partial Y}{\partial r} = 0$	$u = 0$	$\frac{\partial w}{\partial r} = 0$	$\psi = 0(u = 0)$

Table 1: Table of boundary conditions for experimental Domain 1.

Physically speaking, it enforces that no fuel vapors go in or come out of the fritted glass disk. The boundary conditions in Table 1 are those that represent an uncovered fuel pool open to Domain 1. Once the fuel pool is covered by a film layer, the boundary condition for Y on 1 will change to reflect Henry's Law. Henry's Law states that the vapor pressure of a gas is proportional to the amount of that gas dissolved in a liquid.

The first validation test that was performed in the experimental domain was a flux test which involved specifying a flux on the fuel pool surface. This flux boundary condition replaced the boundary condition of $Y = Y_{sur}$. What this specified flux implied was that there was a constant amount of evaporation taking place on the surface. At steady state, the amount of evaporation coming off of the surface would also be coming out of the outlet. The code was run out to steady state to see if it was able to reproduce the evaporation at the outlet. The model was able to do so, which meant that the extra features in the domain were added correctly.

The defining test of the code was to compare it to experimental data. Williams et al performed experiments for an uncovered n-heptane pool with a nitrogen flow rate of $78\frac{cm^3}{min}$. The values for D_A and Y_{sur} were found respectively by using Chapman-Enskog kinetic theory and Antoine parameters. Because of the relatively high flow, there was noise in the experimental value which meant that the uncertainty range was fairly high. The values for the experiment and the numerical model were very comparable though with the experiment measuring a total flow of $110\frac{\mu g}{s}$ and the numerical model predicting $130\frac{\mu g}{s}$. With these test results, it was concluded that the model was working correctly and could

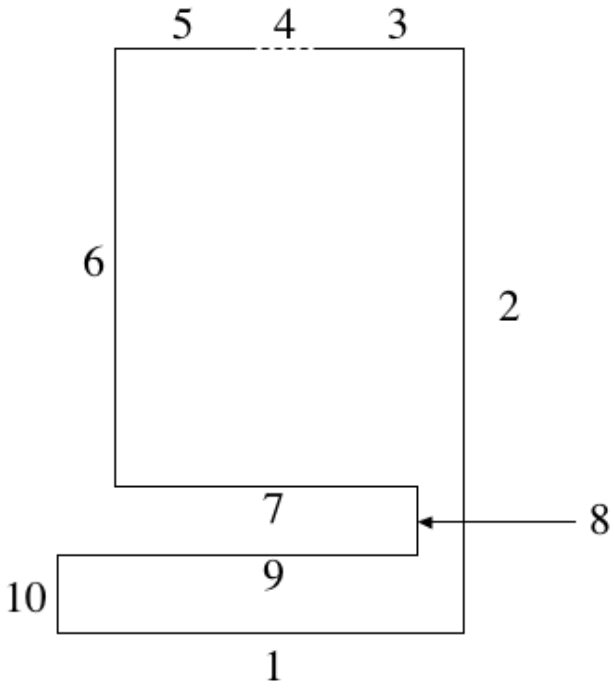

Figure 5: Plot of the experimental Domain 1 with labeled boundaries. These labels correspond to boundary conditions in Table 1.

accurately calculate concentrations and total flow for the uncovered fuel pool case. Before adding the optimization routine, Domain 2 had to be coupled to Domain 1.

Physically speaking, this would result in covering the fuel pool and it changes some of the previously listed boundary conditions. Table 2 is a list of the boundary conditions corresponding to the labeled boundaries in Figure 6. The boundary condition of $Y = Y_{sur}$ on 1 now changes to $Y = \frac{P_v}{P_a} Y_F$ to represent Henry's Law. In this formulation, P_v is the resulting vapor pressure from a pure fuel pool open to air, P_a is the atmospheric pressure, and Y_F represents the fraction of fuel on the surface of the film domain. The boundary condition representing the fuel pool is now on boundary 11, $Y = Y_{sur}$, and Y_{sur} is the mole fraction that results from the solubility of fuel in water. This is an approximation though because the aqueous solution has some amount of surfactant in it. Nonetheless, this approximation will be used and its validity will be analyzed once the model is applied to the data. The last boundary condition that needs to be discussed is that of 13. This boundary condition enforces matching fluxes. The left hand side is the flux on the top surface of the film layer in the film domain and the right hand side represents the flux

Boundary	Y
11	$Y = Y_{sur}$
12	$\frac{\partial Y}{\partial r} = 0$
13	$\rho_F D_F \frac{\partial Y_F}{\partial z} = \rho_A D_A \frac{\partial Y_A}{\partial z}$
14	$\frac{\partial Y}{\partial r} = 0$

Table 2: Table of boundary conditions for experimental Domain 2.

on the top surface of the film layer in the air domain. The subscript A denotes the air domain and the subscript F denotes the film domain. Once coupled, boundaries 13 and 1 will be the same boundary. However, two boundary conditions are needed since it is the demarkation of two domains. Note that no validation is needed for Domain 2 because the species fraction solver has already validated for a pure diffusion case.

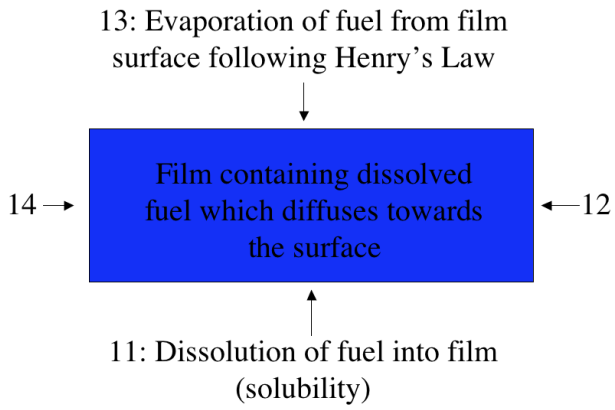

Figure 6: Plot of the experimental Domain 2 with labeled boundaries. These labels correspond to boundary conditions in Table 2.

Optimization Validation

The method that was chosen to minimize the residual between the numerical and experimental data was the secant method. The purpose of the secant method was to find the D_F value that reproduced the experimental data within some tolerance. The data that was provided came in several different forms. For some experiments, the data came in the mole or mass fraction at the outlet for the uncovered and covered case. Other ex-

periments presented the data in the form of a ratio of the two cases. Thus, to create a model that could handle both forms of data, the secant method was designed to operate on the ratio form. In the case when the data was not presented in ratio form a ratio was easily created by dividing the covered value by the uncovered value. The ratio format also had the added benefit of removing some of the experimental uncertainty from the data.

$$D_{F,n+1} = D_{F,n} - (R_{exp} - R_n)\Big(\frac{D_{F,n} - D_{F,n-1}}{(R_{exp} - R_n) - (R_{exp} - R_{n-1})}\Big) \tag{10}$$

The secant method formulation for making the next guess at D_F then took the form of (10), where R_{exp} is the ratio of the experimental data. In (10), R_n and R_{n-1} represent the numerical data ratios that resulted from $D_{F,n}$ and $D_{F,n-1}$ respectively. To form R_n, the uncovered case must be known so the model is run for the uncovered case first. It then stores the value in memory, covers the pool, and proceeds with the covered pool simulations. Because the secant method formulation is being used, two initial guesses at D_F are required. For a foam layer, the initial guesses were made using Chapman Enskog kinetic theory and for a film layer, the Wilke-Chang equation for liquid-liquid diffusion is used. Both Chapman Enskog kinetic theory and the Wilke-Chang equation for liquid-liquid diffusion are presented in [5].

To validate the implementation of the secant method, a test case was created. The test case concerned a $3cm$ high foam layer being placed on a n-heptane fuel pool. The value of D_F was initially set to $D_F = 0.01\frac{cm^2}{s}$ so that the uncovered and covered steady state concentration could be found. The ratio of these two values was set to R_{exp} and the value of $D_F = 0.01\frac{cm^2}{s}$ was removed from the code. Given R_{exp}, the model was asked to find the D_F value that would reproduce $|R_{exp} - R_n| \leq \gamma$ where γ is some tolerance. The model correctly reproduced $D_F = 0.01\frac{cm^2}{s}$ for the value of R_{exp} so the secant method was known to be implemented correctly.

5 Results

Application to Test Data

The first case run with the fully coupled, optimization capable, model was for a n-octane pool covered by $1cm$ of film. The flow rate of N_2 into the container was $630\frac{cm^3}{min}$ and at $100s$ the concentration was measured to be 0.15% of the uncovered value. To find the diffusion coefficient for n-octane in N_2, D_A, Chapman-Enskog kinetic theory was used. This resulted in an estimate of $D_A = 0.06\frac{cm^2}{s}$. As a check on the validity of using this kinetic theory, D_A for n-octane in N_2 was compared to experimentally determined values, which were within 3% of D_A. The concentration boundary condition that was used on boundary 11 was a mole fraction value of 0.018 and the boundary conditions used on boundary 1

was Henry's law, $0.018Y_F$ ($\frac{P_v}{P_a} = 0.018$ for n-octane). Using these input parameters and data, the model found that $D_F = 1.36 * 10^{-3} \frac{cm^2}{s}$ was the diffusion coefficient responsible for the experimental measurements. Figures 7 and 8 are contour plots of the axial and radial velocities within the container at a time of $100s$. Figures 9 and 10 are contour plots of the concentration (mole fraction) of fuel vapors within Domains 1 and 2 at $100s$.

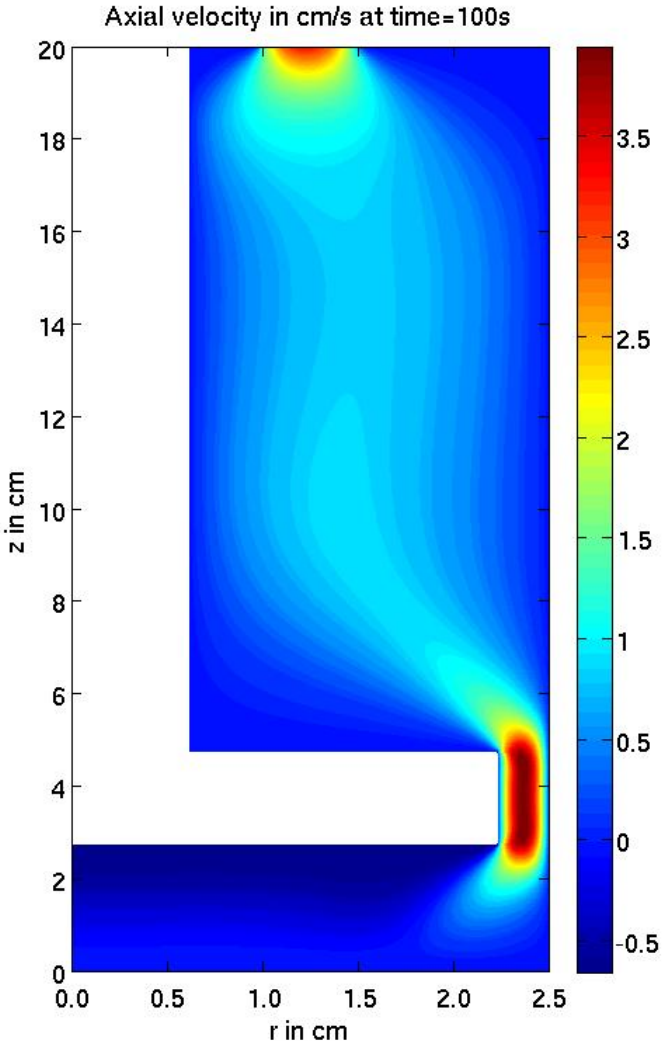

Figure 7: Contour of the axial velocity inside Domain 1 at $100s$ resulting from an N_2 input flow of $630 \frac{cm^3}{min}$.

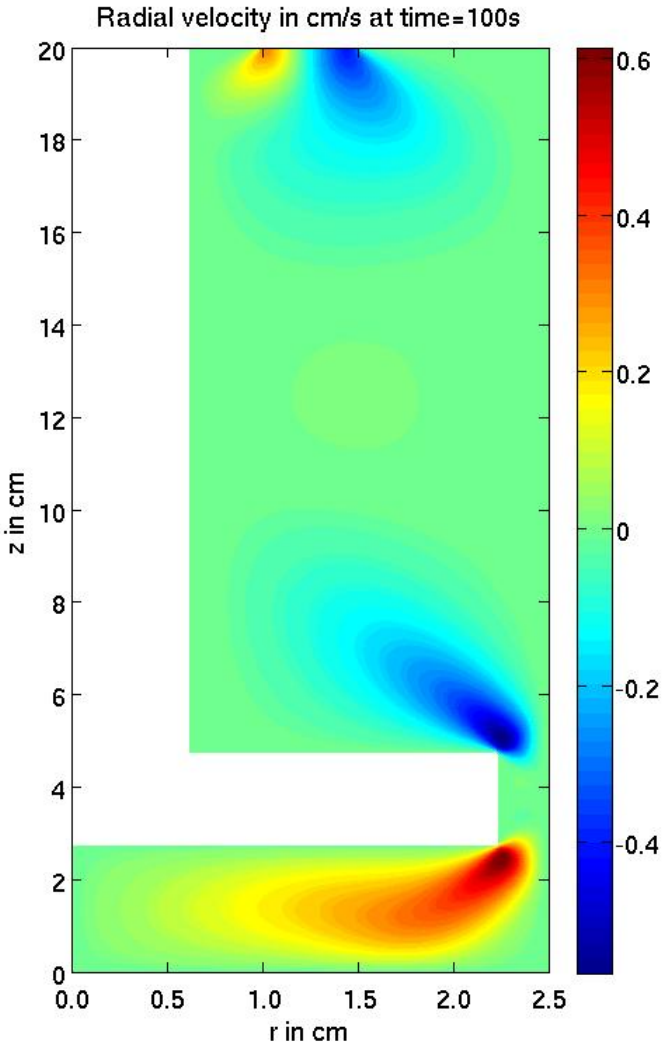

Figure 8: Contour of the radial velocity inside Domain 1 at $100s$ resulting from an N_2 input flow of $630\frac{cm^3}{min}$.

Application to Film Data

The first case that the model was run on was a set of test data. This case was created to show that the model was capable of modeling the experiments and finding the D_F value responsible for the data. Once the model is applied to actual experimental data,

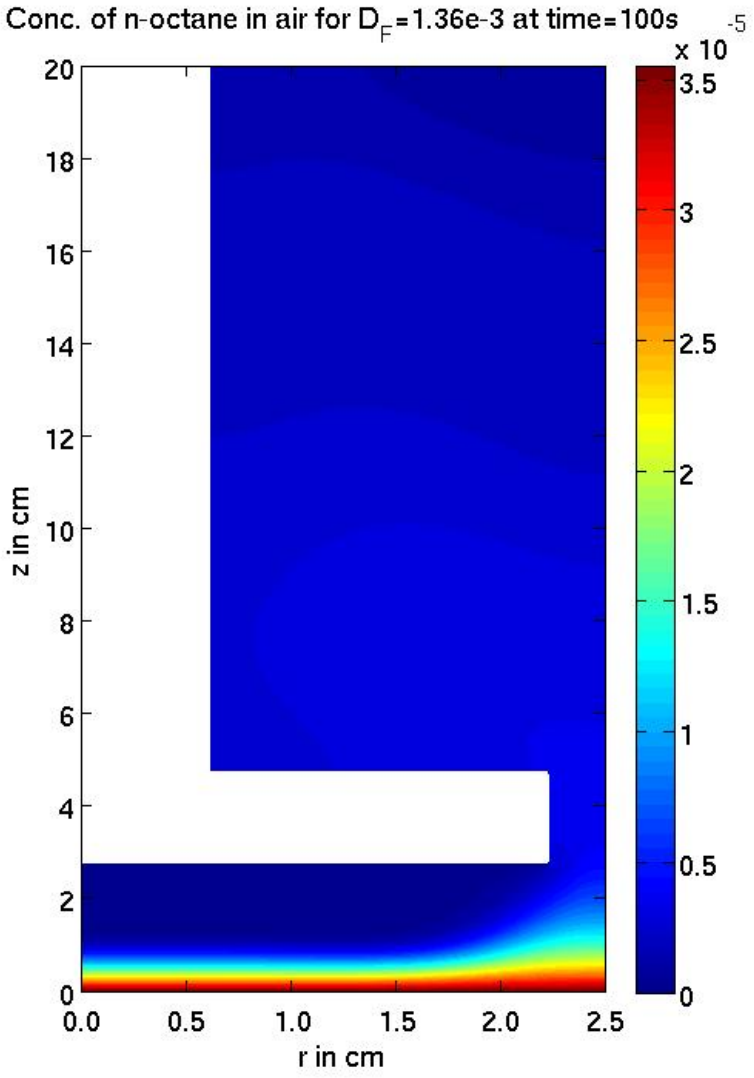

Figure 9: Contour of the fuel vapor concentration inside Domain 1 at $100s$ resulting from $D_F = 1.36 * 10^{-3} \frac{cm^2}{s}$.

it produces very interesting results. The actual experimental data that the model was run on was the film layer data gathered by Leonard. The model was not run on the foam layer data gathered by Williams because the data appears to have a conversion factor error. Thus, the model was run on the credible data that was immediately available.

One experiment that Leonard ran was for a n-octane pool covered by $2.35 * 10^{-3} cm$

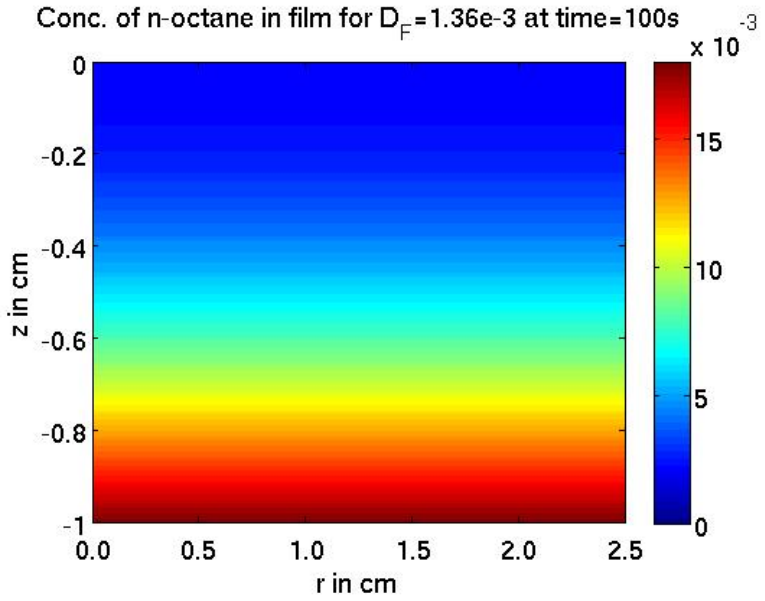

Figure 10: Contour of the fuel vapor concentration inside Domain 2 at $100s$ resulting from $D_F = 1.36 * 10^{-3} \frac{cm^2}{s}$.

of film. The flow rate of N_2 was $630 \frac{cm^3}{min}$ and at $1800s$ the concentration (mole fraction) was measured to be 15% of the uncovered value. The boundary condition used on boundary 11 was $3 * 10^{-7}$. This value is the actual solubility of n-octane in water as opposed to the value of 0.018 that was used in the test case. The boundary condition of Henry's Law, $0.018 * Y_F$, is valid for boundary 1 since $\frac{P_v}{P_a} = 0.018$ for n-octane and it was applied.

The first guess of the film layer diffusion coefficient was $D_{F,1} = 1 * 10^{-5} \frac{cm^2}{s}$. Figure 11 is a plot of the concentration (mole fraction) of fuel vapors at the outlet versus time. There are two features of Figure 11 that need to be noted. The first of which is that the steady state of fuel vapors at the outlet is reached within $70s$ for this value of $D_{F,1}$. Changing the value of D_F will only change the amount of time needed to reach steady state and would not change the concentration of fuel vapors at steady state. The concentration magnitude is the second feature that needs to be noted. At steady state, the concentration of fuel vapors is on the order of 10^{-9}, while the uncovered concentration was found to be $2.35 * 10^{-3}$. Taking the ratio of these values we see that $R_1 = 3 * 10^{-6}$.

Comparing these results to Leonard's data, one can see that the time scale and ratio are both several orders of magnitude away from the numerical results. Figure 12 is a further illustration of this point, with Leonard's data and the numerical results for $D_{F,1} = 1 * 10^{-5} \frac{cm^2}{s}$ plotted on the same graph. If the model was allowed to optimize over D_F, it would have "guessed" lower and lower values for D_F. This would have the effect

of increasing the amount of time to reach steady state, however, this would require values much smaller than 10^{-9}. A diffusion coefficient lower than this value would be consistent of that of solid-solid diffusion so we can see that values of this order of magnitude would be unreasonable. Changing D_F would also have no effect on changing the concentration value at steady state. With these two things in mind, it was decided to perform some analysis on the solution to see what could be responsible for the discrepancies.

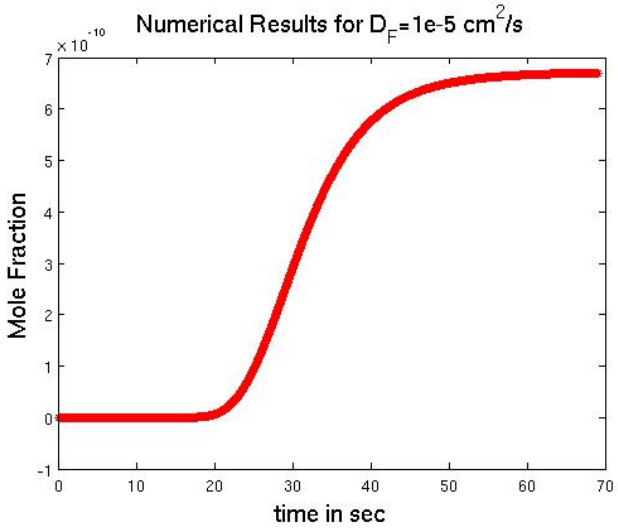

Figure 11: Plot of the fuel vapor concentration at the outlet versus time for $D_F = 1 * 10^{-5} \frac{cm^2}{s}$.

Analysis of Results and Leonard's Data

In his experiment, Leonard measured a concentration corresponding to 15% of the uncovered case at $1800s$. The concentration profile at the outlet at $1800s$ for the uncovered case is $Y = 2.35 * 10^{-3}$. Taking 15% of that value leaves us with a measurement of $Y = 3.525 * 10^{-4}$ for the covered case at $1800s$. Noting that in Figures 9 and 10, the concentration increases as height decreases, one can expect the same phenomena in this case. Thus, in Domain 1, at the film layer surface, one would expect $Y > 3.525 * 10^{-}4$. Applying Henry's Law, this time in the opposite direction, one can see that in Domain 2 at the film layer surface $Y_{sur} > \frac{3.525*10^{-4}}{0.018}$. Again, as height decreases, the concentration on fuel vapors will increase, so at the surface of the fuel pool one would expect $Y_{sol} > Y_{sur}$. This implies that Y_{sol}, the mole fraction due to the solubility of n-octane in the aqueous solution, will have to be larger than $\frac{3.525*10^{-4}}{0.018}$, or approximately 2%. Remember that the original solubility that was used in this model was $3 * 10^{-7}$. Thus, one can see that there is a clear disagreement in the boundary conditions and one that could account for the

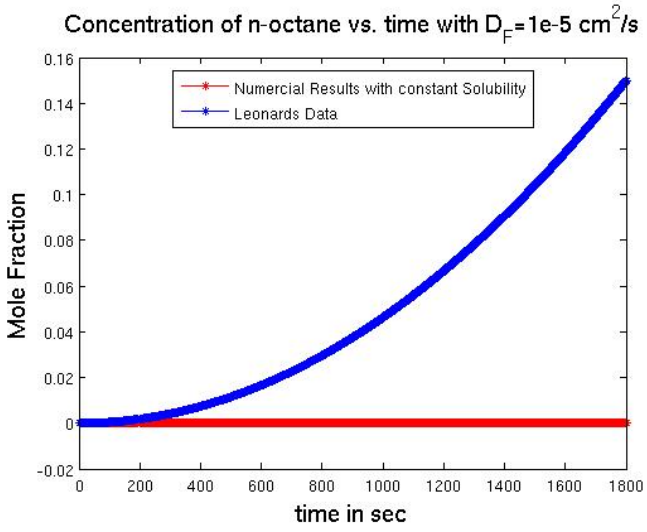

Figure 12: Comparison of Leonard's experimental data and the numerical results for an initial guess of $D_F = 1 * 10^{-5} \frac{cm^2}{s}$. Plot of the fuel vapor concentration at the outlet versus time.

previous discrepancies between Leonard's experimental results and the numerical results.

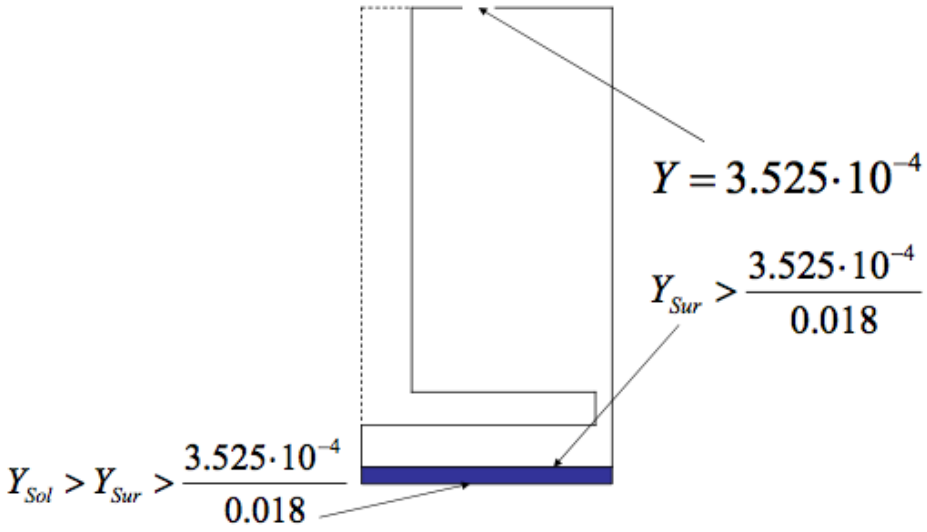

Figure 13: Analysis of mole fraction in Leonard's experimental data.

The model has been extensively validated and it is known that the model correctly predicts the uncovered fuel pool case. The results captured in Figures 11 and 12, along with the above analysis, suggest that the assumption of dissolution and diffusion of fuel vapors in the film layer is not valid. This is due to the fact that a very high solubility of n-octane in the aqueous solution is necessary in order to reproduce Leonard's data. At this point, one cannot rule out a time dependent boundary condition for Y_{sol} nor a time dependent diffusion coefficient D_F. Time dependence on Y_{sol} and/or D_F could be responsible for the large time scale observed in Leonard's data while still allowing for a dissolution and diffusion transport mechanism. Currently, emulsification is being looked at as the transport mechanism because of the short comings of the dissolution and diffusion mechanism highlighted by this model. In order to try to dispel notions of dissolve and diffuse, experiments are being planned to measure the solubility of fuel vapors in the aqueous solution. If the solubility is unable to reach a value of 0.02% or higher, then it will be clear that another mechanism must be responsible for the transport of fuel through the film layer. At the same time, plans for rerunning the foam layer experiments are underway so that the model can be applied to the data. It will be interesting to see if a similar discrepancy appears in the foam layer simulations. In the immediate future, the model will be run with $Y_{sol} \geq 0.02$ to find the effective D_F value that is capable of reproducing Leonard's results.

6 Conclusions

At the start of this project, I said that I would deliver a software package that modeled the experiments of Leonard and Williams by assuming the dissolution and diffusion transport mechanism. This software package was also to be capable of finding an effective diffusion coefficient D_F for a film or foam layer. The value of D_F would be found by minimizing the residual between the experimental and numerical results. Unfortunately, the foam data that was originally promised was corrupted so the model was only able to be run on the film layer data. Nonetheless, the model that has been created is entirely capable of simulating a foam layer. In addition to the software package, I said that I would deliver my input data and it has all been presented in this paper. In addition to my deliverables, I have also presented findings that suggest that emulsification is the mechanism responsible for transporting the fuel through the film layer.

7 References

1. Leonard, J.T., and Burnett, J.C. "Suppression of Fuel Evaporation by Aqueous Films of Fluorochemical Surfactant Solutions". NRL Report 7247. 1974

2. Williams, B.A., Murray, T., Butterworth, C., Sheinson, R.S., Fleming, J., Whitehurst, C., and Farley, F. "Extinguishment and Burnback Tests of Fluorinated and Fluorine-free Firefighting Foams with and without Film Formation." Suppression, Detection, and Signaling Research and Applications- A Technical Working Conference (SUPDET 2011). March 22-25, 2011. Orlando, Florida.

3. Williams, B.A, Sheinson, R.S., and Taylor, J.C. "Regimes of Fire Spread Across an AFFF – Covered Liquid Pool". NRL Report. 2010

4. Ananth, R, and Farley, J.P. "Suppression Dynamics of a Co-Flow Diffusion Flame with High Expansion Aqueous Foam". Journal of Fire Sciences. 2010

5. Bird, R.B., Stewart, W.E., and Lightfoot, E.N. *Transport Phenomena.* John Wiley and Sons. 1960

6. Pozrikidis, C. *Introduction to Theoretical and Computational Fluid Dynamics.* Oxford University Press. 1997

7. Panton, R.L. *Incompressible Flow.* John Wiley and Sons. 1984.

8. Press, W.H., Teukolsky, S.A., Vetterling, W.T., Flannery, B.P. *Numerical Recipes in Fortran.* Cambridge University Press. 1992